

# MOEMS micromirror arrays in smart windows for daylight steering

Hartmut Hillmer,\* Mustaqim Siddi Que Iskhandar<sup>ORCID</sup>,  
Muhammad Kamrul Hasan, Sapida Akhundzada,  
Basim Al-Qargholi, and Andreas Tatzel

University of Kassel, Institute of Nanostructure Technologies and Analytics,  
Center for Interdisciplinary Nanostructure Science and Technology, Kassel, Germany

**Abstract.** Micro-opto-electro-mechanical systems (MOEMS) micromirror and shutter arrays have gained huge interest in research and applications. Our study starts with an overview on the technological achievements and experimental results of groups that have been working on this field. The main part of our study is revealing the MOEMS micromirror array technology for light steering via smart glazing for buildings. The mirror array is actuated electrostatically and integrated between the panes of insulation glazing. Depending on user activity as well as daytime and season requirements, the MOEMS micromirror arrays shall enable personalized light steering, energy saving, and reduction of CO<sub>2</sub> emission. Technological fabrication of subfield addressing up to 64 fields inside the arrays is presented. Experimental characterization results such as actuation voltages, maximum and minimum transmission, contrast, and energy saving potential are reported. Using an industrial window module fabrication process, a laboratory demonstrator and a function demonstrator have been implemented. Rapid aging tests including vibrations, extreme temperatures, multiple temperature cycles, and long-term electrostatic actuation of micromirror structure were performed to evaluate reliability and lifetime. These results validate extrapolated lifetimes—in future applications as active windows—far beyond 40 years, as well as their robustness during transportation, installation, and against all vibration influences in buildings. © The Authors. Published by SPIE under a Creative Commons Attribution 4.0 Unported License. Distribution or reproduction of this work in whole or in part requires full attribution of the original publication, including its DOI. [DOI: [10.1117/1.JOM.1.1.014502](https://doi.org/10.1117/1.JOM.1.1.014502)]

**Keywords:** micro-opto-electro-mechanical systems; micromirror array; light steering; daylight; subfield addressing; smart window; buildings.

Paper 20015 received Sep. 29, 2020; accepted for publication Nov. 30, 2020; published online Jan. 26, 2021.

## 1 Introduction

Micro-opto-electro-mechanical systems (MOEMS) for light processing have been fabricated and studied for various applications. Micromirror array-based MOEMS have been reported for  $N \times N$  switches in wavelength division multiplexing,<sup>1–3</sup> beamers,<sup>4,5</sup> light steering via smart glazing for buildings,<sup>6,7</sup> and adaptive optics.<sup>8,9</sup> In adaptive optics, the applications are high-order correction of optical aberrations to be used in astronomy, maskless lithography, microscopic medical technology, laser micromachining, and optical free space communication. These MOEMS mirror elements are planar and are actuated electrostatically. Note that some adaptive optics are based on freeform reflectors.<sup>10,11</sup> The mirror arrays for switches and beamers<sup>1–5</sup> are Si-based and the mirrors are automatically planar by MOEMS standard processing. The mirrors for light steering in smart glazing are metal-based<sup>6,7</sup> and nearly planar due to partial stress compensation.

Likewise, metal-based but in the relaxed state nonplanar (i.e., curled/rolled), in contrast, are optical MEMS that are usually called shutter arrays<sup>12–17</sup> or microblinds.<sup>18</sup> Shutter-array-based MOEMS have been reported for transmission modulated smart glass,<sup>12,18</sup> space instrumentation,<sup>13</sup> camera shutters,<sup>15</sup> and displays.<sup>16,19</sup> These MOEMS shutter arrays are curled in the open state and unrolled by electrostatic actuation to obtain the flat closed condition. One type of these

---

\*Address all correspondence to Hartmut Hillmer, [hillmer@ina.uni-kassel.de](mailto:hillmer@ina.uni-kassel.de)

MOEMS is shutter systems defined as rolled elements found in many different application fields. Pizzi et al.<sup>16</sup> developed curled microshutter arrays aiming at low-cost applications and a replacement of infrared (IR) photodetector arrays. A similar system designed by Mori et al.<sup>20</sup> is electrostatically reconfigurable microshutter arrays implemented between window planes for modulating incoming sunlight. In all these microshutter arrays, each shutter moves/behaves as the neighboring one.

Recently, Lamontagne et al.<sup>21</sup> published a laboriously researched review article on microshutters giving a valuable overview about that class of technology. This review also included our micromirror arrays. We take the opportunity to update the tables of Lamontagne et al. and present it in Table 1. For our smart micromirror glazing, we measured a minimum transmittivity  $T_{\min}$  of 0.01%<sup>7</sup> and recently a maximum transmittivity  $T_{\max}$  of 73%, yielding a modulation contrast of  $T_{\max}/T_{\min} = 7300$  between open and closed states. The rest of this paper is organized as follows: Section 2 presents foundations of our smart glass technology based on MOEMS micromirror arrays and depicts different application scenarios. The technological fabrication is described in Sec. 3 focusing on subfield addressing. Section 4 presents electrical and optical characterization of the MOEMS arrays. Section 5 presents the implementation of a laboratory and a function demonstrator. Extensive experimental reliability and lifetime tests are reported in Sec. 6. Finally, our MOEMS technology is compared to different state-of-the-art shading systems in Sec. 7.

## 2 Methodology of MOEMS Micromirror Arrays for Smart Glazing

The sustainable design of “smart green buildings” has become increasingly important for limiting global warming and carbon dioxide emission reduction via efficient energy saving. The implementation of efficient daylighting strategies can considerably reduce energy consumption in buildings since artificial light, cooling, and heating constitute today about 40% of the global total energy consumption in buildings and cause a third of the global total CO<sub>2</sub> emission. In addition, daylight instead of artificial light is of major importance for the human biorhythm, health, learning success, and minimization of error susceptibility. In winter, daylight directs favorable thermal energy into the buildings. However, daylight is also accompanied by uncomfortable solar glare and reflections on display screens, both of which interfere with optimum vision. Until now, no smart glass technology can actively adapt to all requirements without significant disadvantages.

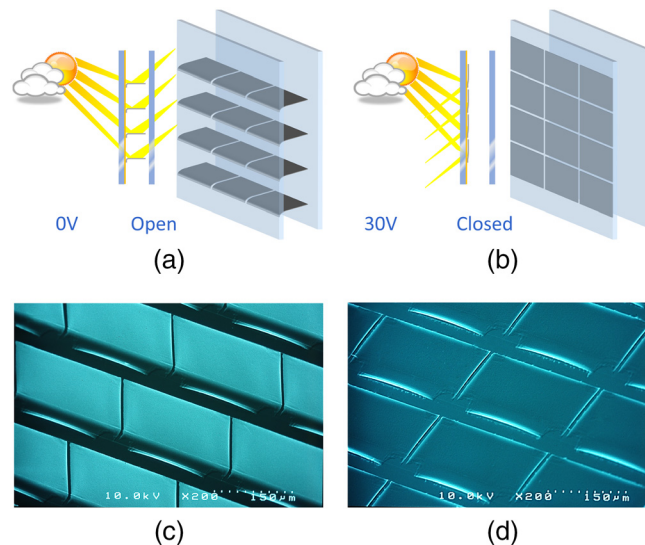
3D micro- and nanostructured mirror arrays for daylight guiding<sup>6,7</sup> comprise millions of electrostatically actuatable micromirrors that can guide and control light dynamically by tailored reflection (Fig. 1). The micromirror structure is implemented by a hybrid metal multilayer system with individual thicknesses between 10 and 100 nm in vertical direction and mirror sizes of typically  $150 \times 400 \mu\text{m}^2$  in lateral direction. The micromirrors are miniaturized so that the naked eye cannot identify them from a distance of more than 20 cm from the array. Thus, an impression of a variable-tone pane is obtained. They are invulnerable to wind, window cleaning, or any weather conditions since the mirror array is located in the space between the windowpanes filled with noble gas such as argon or krypton. Applications in cars, aircrafts, and trains are also possible, however, at the moment car industry refuses double glazing due to weight problems and cost since the double panes need to be bent, arbitrarily.

Figure 2 displays a schematic cross section of four application scenarios. In each scenario, the window part (middle) is denoted by two blue glass pane with white space filled with insulating gases and the micromirror arrays are visualized by strongly magnified lines/bars. The left side of the window shows different sun positions in the sky, and the right side is a room inside a building. The four different scenarios describe summer or winter situations as well as user’s presence or absence. This concept is flexible to confront different situations (location on earth, window orientation, day- and night-time, season, number of floors, and tilt angle of panes) and any possible user action as follows.

- (a) If no user is present inside the room in summer (very high solar impact), the smart glazing will close by switching all the micromirrors vertically. This reflects the whole solar radiation to the outside and the room stays cool, automatically. This saves huge energy for climatization by minimizing heat transfer into the room.

**Table 1** MOEMS shutter technology comparison of different research groups (update of Ref. 21): materials, size of single-shutter elements, experimental properties, and potential applications

| Research group       | Reference | Time            | Bottom electrode               | Top electrode                            | Size   | Actuation (V) | Speed to close              | Demo. size                 | Max/min transmission % to contrast | Applications, comments   |
|----------------------|-----------|-----------------|--------------------------------|--|--|---------------|-----------------------------|----------------------------|------------------------------------|--|
| Fiat                 | 16 and 17 | 1999 to 2005    | ITO                            | flexible metal layer                     | 458 $\mu\text{m}$ to 2.4 mm  | 20 to 100     | 0.1 ms                      | —                          | 20/1 to 20                         | Microshutter-based automotive display, IR spectrometry, low transmission |
| MCNC                 | 22        | 2000 to 2002    | ITO                            | polyimide/Cr/Au/polyimide                | <100 $\mu\text{m}$ to over 200 $\mu\text{m}$                             | 100 to 300    | 18 $\mu\text{s}$            | 5 $\text{cm}^2$            | Low contrast                       | Eyelid for protection  |
| Kassel University    | 6 and 7   | 2003 to present | ITO, FTO or Ag low-e           | $\text{SiO}_2\text{-SiN}_x/\text{Al-Cr}$ | 150 $\times$ 400 $\mu\text{m}^2$   | 12 to 40      | 0.33 ms                     | Almost 1000 $\text{cm}^2$  | 73/0.01 to 7300 high contrast      | Sunlight steering for buildings, high contrast, low voltage              |
| NRC                  | 18 and 21 | 2005 to present | $\text{SnO}_2$ , ITO, Ag low-e | Cr and others                            | 50 to 300 $\mu\text{m}^2$  | 15 to 25      | 40 $\mu\text{s}$            | 20 $\text{cm}^2$           | 60/0.1 to 600 high contrast        | High contrast, low voltage   |
| NVMG                 | 12 and 14 | 2007 to present | TCO                            | shrinkable Polymer                       | $\geq 2$ mm  | 100 to 500    | in seconds                  | 5000 $\text{cm}^2$         | Low contrast                       | Macrocurling shutter, commercialized                                     |
| INO                  | 13 and 21 | 2008 to 2009    | Al                             | MoCr                                     | 60 $\times$ 1000 $\mu\text{m}^2$   | 110           | 2 ms to close, 7 ms to open | 0.25 $\text{cm}^2$         | Low contrast                       | Space instrumentation  |
| Air Force            | 23        | 2008            | AlZnO                          | Ti and Au                                | 200 $\times$ 50 $\mu\text{m}^2$  | —             | —                           | —                          | 40/1 to 40                         | Adaptive coded aperture imaging  |
| Samsung              | 15 and 24 | 2009 to 2011    | ITO                            | Al-SiN <sub>x</sub> , Mo-Mo              | $\varnothing$ 2.2 mm, 36 $\times$ 1.4 mm long triangular rolled shutters | 30            | 2 ms                        | Iris of 0.04 $\text{cm}^2$ | ?                                  | Iris shutter for camera  |
| KAIST                | 25 and 26 | 2010 to 2016    | ITO                            | Electroplated Ni                         | 200 $\times$ 160 $\mu\text{m}^2$   | 20 to 30      | 20 $\mu\text{s}$ to close   | Small                      | 60/? to ?                          | Active transparent display with TR-OLEDs                                 |
| University of Tokyo  | 20        | 2015 to 2016    | ITO                            | Al-SiO <sub>2</sub>                      | 200 $\times$ 30 $\mu\text{m}^2$  | 38 to 55      | 3 ms                        | —                          | 53/36 to 1.5                       | Implemented on TFT   |
| Stuttgart University | 19 and 27 | 2016 to present | MoTa                           | MoTa on stressed SiN <sub>x</sub>        | 200 $\mu\text{m}$  | 20 to 60      | —                           | 2 to 225 $\text{cm}^2$     | Low contrast                       | Transmissive display on TFT, low transmission                            |



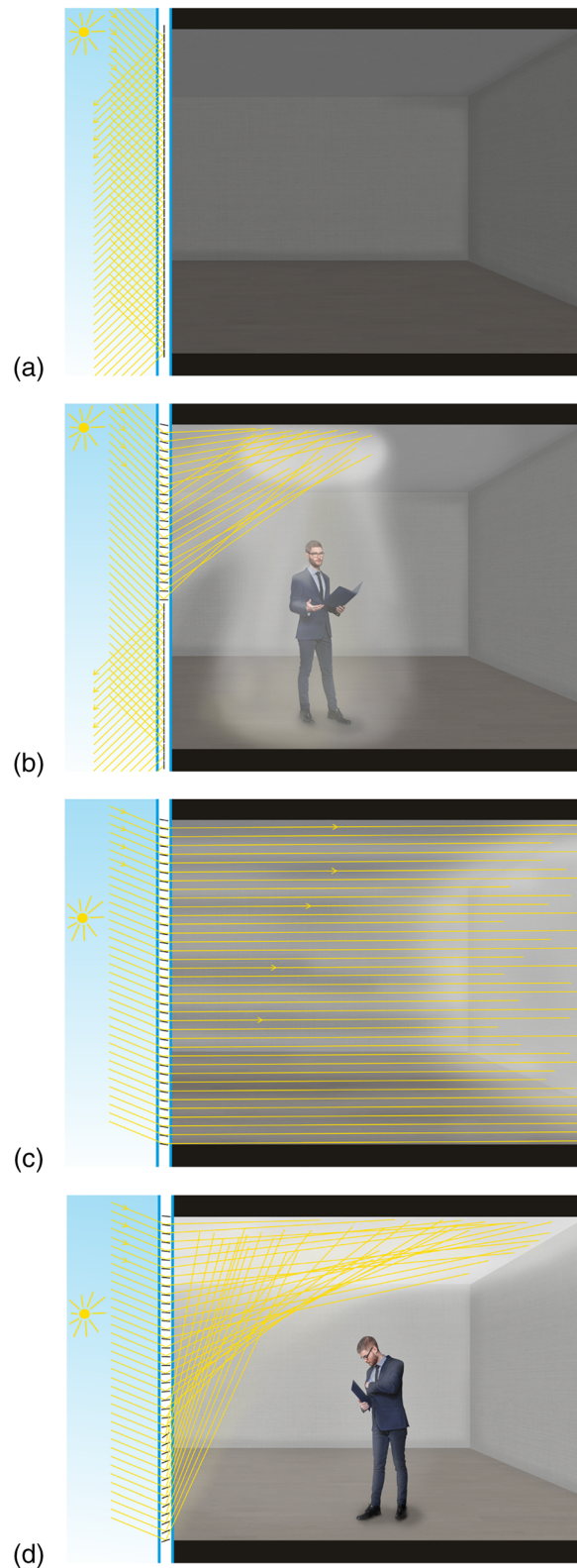
**Fig. 1** Micromirrors in open and closed scenario, shown in (a), (b) schematics and (c), (d) SEM micrographs, respectively. The smart glass pane is integrated into a double insulation glazing in Ar atmosphere and sealed by butyl.

- (b) Once user presence is detected by sensors in summer, the upper mirrors open and reflect daylight onto a limited ceiling area above the user in the room. The lower window part still stays in a closed position and still reflects the solar radiation to outside. Thus the room stays cool where no user is standing. In a final implementation, the light spot on the ceiling moves with the user automatically. This still saves a lot of energy for climatization since heat transfer is limited to a small amount. In addition, parts of the room far away from the window can be efficiently illuminated by daylight. This saves the energy needed for artificial light.
- (c) If no user is present in winter, all the mirrors open and efficiently harvest energy, reflecting the whole solar radiation onto a central wall, subsequently acting as a radiation heater. This saves huge energy needed for heating.
- (d) Once user presence is detected in winter, all the mirrors will redirect the complete solar radiation to the ceiling to minimize glare. Now, the ceiling acts as a radiation heater, saving heating energy. Contrarily, conventional blinds are often lowered in winter due to glare caused by low sun position requiring artificial lighting (unnecessary energy consumption, unhealthy, missing to harvest natural heat, and daylight use).

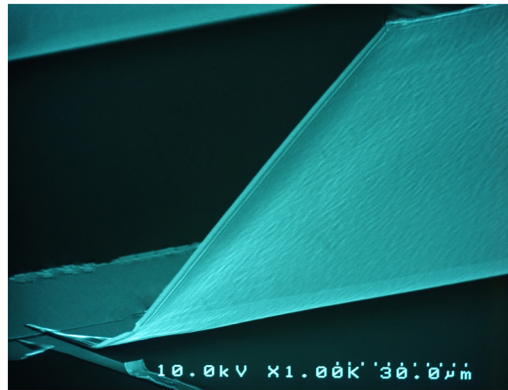
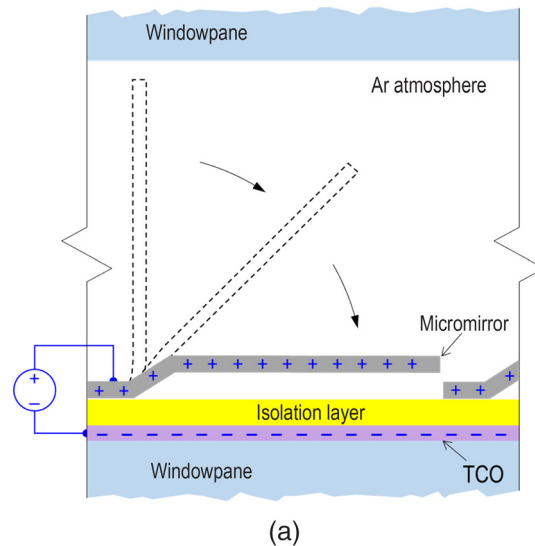
In all scenarios, room temperature and lighting settings will be regulated automatically: energy consumption through artificial lighting, fans, air-conditioning, and heating systems can be curbed. This provides huge impact on energy efficiency, economy, health, and society.

### 3 Technological Fabrication Focusing on Subfield Addressing

Figure 3(a) shows a schematic of a single-mirror actuator in inert gas atmosphere (typically argon) between the two panes of a double insulation glazing. Each mirror consists of a flat mirror plane, the bent hinge, and a supporting post attached to the glass pane. Figure 3(b) depicts an SEM micrograph of a free standing, planar mirror. During micromachined fabrication, the sacrificial layer is removed in a wet chemical process. Due to the intrinsic layer stress in the multilayer stack, the uncompensated hinge region strongly bends and lifts the mirror to a vertical position. The mirror area is stress compensated, resulting in planar mirror areas. The electrostatic actuation voltage is applied between the whole metal multilayer stacks (consisting of supporting post, hinge, and mirror), which is shown in gray and the transparent conductive electrode layer on the pane, depicted in purple. The transparent conductive electrode layer is implemented either by transparent conductive oxides (TCO) such as indium tin oxide (ITO) and fluorine-doped tin



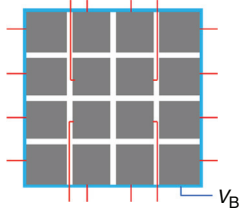
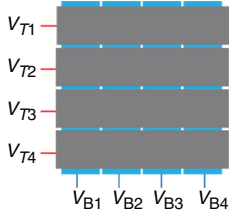
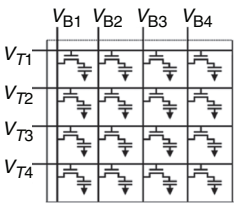
**Fig. 2** Scenarios of a room with or without persons present. Schematic sun ray tracing is depicted for four different scenarios: (a) summer, absent user: sun radiation is reflected back and the room is not heated; (b) summer, user present: since only a part of the light is reflected to the ceiling, the heating of the room is limited; (c) winter, absent user: the solar IR is completely used and heats a wall; and (d) winter, user present: all the visible and IR radiation is reflected to the ceiling.



**Fig. 3** (a) Schematic of the electrostatic actuation of a single mirror. (b) SEM micrograph of a flat, free-standing micromirror.

oxide (FTO), or by 5-nm-thick Ag layer included in low-emissivity (low-e) coatings. The two electrodes are separated by a  $\text{SiO}_2$  isolation layer (yellow). By varying the potential difference between these electrodes, several opening angles can be achieved via the equilibrium in the moments of force between electrostatic attraction and elastic repulsion before the mirrors closes abruptly due to the pull-in effect. The technological MEMS process has been described in previous publications.<sup>6,7</sup> The layer stack consists of sandwiched Al–Cr–Al, typically with 60 to 100 nm of Al and 10 to 40 nm of Cr. The flat mirror configuration requires an additional Al layer of 70 to 120 nm. These values are subject to process type, deposition rate, and the desired opening angle. Depending on the layer stress in the hinge and its extension vertical to the axis, different opening angles can be adjusted. In this paper, we focus on the implementation of subfield addressing.

The integration of subfield addressing scheme into the micromirror array is deemed necessary to allow more control of open and closed area of the smart window. Such a feature is important to implement the envisioned tailored ambient lighting and will further expand the usability and application area, at the same time increasing the appeal for potential utilization. The subfield addressing is implemented by adaptation of a passive matrix scheme (PM scheme)—a common driving scheme in visual display technology—into the multilayer stack of micromirror array. The PM driving scheme is selected due to the lesser manufacturing complexity against active matrix (AM) driving scheme and the suitability with our envisioned application far below the established limitation by Alt and Pleshko<sup>28</sup> at a resolution of  $320 \times 240$  pixels. Both PM and AM

| Driving scheme | Direct  | Passive matrix (PM)   | Active matrix (AM)  |
|----------------|---|---|---|
| Schematic      |  |  |                                      |
| Connection     | Top electrode = 16<br>Bottom electrode = 1<br>Total = $(M \times N) + 1 = 17$     | Top electrode = 4<br>Bottom electrode = 4<br>Total = $M + N = 8$                  | Top electrode = 4<br>Bottom electrode = 4<br>Total = $M + N = 8$  |
| Fabrication    | Patterning of micromirror layer, <b>placement of the connection lines</b>         | Structuring of micromirror layer and FTO layer into rows and columns              | Structuring of micromirror layer and FTO layer into rows and columns, <b>incorporation of TFT as switching element.</b> |

**Fig. 4** Comparison of potential driving schemes to be adapted in micromirror arrays. The schematics are translated into  $4 \times 4$  matrix arrangements of micromirror arrays on a  $10 \text{ cm} \times 10 \text{ cm}$  substrate. Top electrodes (micromirror layer) are depicted as gray with red connection lines, whereas the bottom electrodes are depicted as blue with blue connection lines. Disadvantages are highlighted as text in red. Schematic for AM is modified from Blankenbach, Hudak, and Jentsch.<sup>29</sup>

schemes have the same matrix arrangement of electrodes, and their difference lies in the incorporation of nonlinear switching elements, typically TFT, for each subfield. This has the advantage of higher contrast ratio and resolution but at the expense of higher fabrication complexity and cost. Since the subfield requirement of our smart window application is envisioned toward large grouping of micromirrors for tailored light guiding, such high resolution in the range of modern flat panel displays is not required, thus the complex fabrication process and cost can be saved. Another common and much simpler alternative, namely the direct driving scheme, is not suitable due to its increasing complexity to place the direct connection lines to each subfield, since the connection lines are not easily concealable and will impair the view through the windowpane. This will be more severe for higher subfield numbers since for a given  $M \times N$  scheme the required connection lines for direct driving is given by  $(M \times N) + 1$  as opposed to only  $M + N$  for both PM and AM driving schemes. Considering a micromirror array module with  $4 \times 4$  matrix arrangement as an example, a comparison between the three common driving schemes is summarized in Fig. 4.

The adaptation of driving scheme from visual display technology is feasible due to the similarity of the layer system in micromirror arrays and that of liquid crystal display (LCD), consisting of two separated, vertically adjacent electrode layers. However, it is important to note that the active elements in both systems are clearly different. In LCDs, the active element is the liquid crystal material sandwiched between both electrodes, which can be oriented via the applied potentials. On the other hand, the active element in the micromirror array is the movable micromirror layer, which is also the top electrode itself. The micromirrors, which are in open position by default and are separated from the bottom electrode by an isolation layer (typically  $\text{SiO}_2$ ), can be pulled down (closed) by the attractive electrostatic force resulting from the applied voltage between the electrodes.

The integration of subfield addressing in the micromirror arrays requires both top electrodes (micromirror layer) and the transparent bottom electrodes to be structured in perpendicular arrangements to each other. The glass substrate used for the fabrication is procured with around 650 nm FTO layer as the transparent bottom electrode. The patterning of the FTO layer is executed by wet chemical etching using zinc powder and hydrochloric acid (HCl) as metal-acid etch process and iron (III) chloride ( $\text{FeCl}_3$ ) solution as oxidation and penetration control agent [Fig. 5(a)]. First, an etch mask is fabricated using photoresist MicroChemicals AZ 1518 with layer thickness of  $1.8 \mu\text{m}$ . In order to ensure good photoresist adhesion to the substrate, an additional hard bake at  $145^\circ\text{C}$  for 5 min after the development process is implemented.

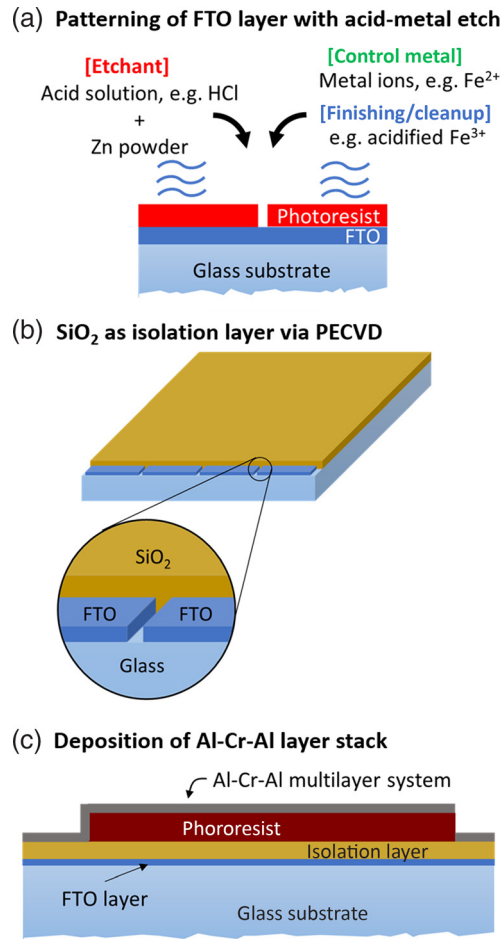


**Fig. 5** Graphic representation of (a) the FTO patterning process with acid-metal etch; (b) deposition of SiO<sub>2</sub> isolation layer with opening at edges for contact area of the bottom electrodes (structured FTO layer); and (c) the deposition of metal layer stack on sacrificial photoresist layer. Free-standing micromirror layer is achieved via removal of the sacrificial photoresist layer.

A good photoresist adhesion is required to avoid undesired etching under the photoresist area (underetching) that can result in insufficient structuring quality of the FTO layer, thus impairing the stability of micromirrors fabricated in the following process steps. Once the etch mask is ready, the area to be etched is sprinkled with enough Zn powder since the etch process will occur locally. The sample is then submerged in an etching solution made of 1.27 M HCl and 0.02 M FeCl<sub>3</sub> for 60 s, rinsed shortly with deionized water to stop the etch process and remove any residual Zn powder, and subsequently submerged in cleaning solution made of 1.26 M HCl and 0.03 M FeCl<sub>3</sub> for at least 5 min to remove the remaining tin (Sn) and the reduced penetration control metal. The structuring process of the FTO layer as bottom electrode is finalized by the removal of the photoresist etch mask using stripper solution such as dimethyl sulfoxide at 80°C for 5 min.

Prior to the fabrication of micromirror layer, SiO<sub>2</sub> is first deposited by PECVD process as an isolation layer. About 4 mm area from the edges are left free of SiO<sub>2</sub>, allowing connection to the bottom electrodes [Fig. 5(b)]. This is followed by the optical lithography process to pattern the sacrificial photoresist layer according to the micromirror design. The patterning of top electrodes into separate rows is defined in this step, and the rows must be aligned with the bottom electrodes (in columns) to obtain uniform subfield size across the module. The 4 × 4 matrix arrangement on 10 cm × 10 cm substrate resulted in about 22 mm × 22 mm subfield size consisting of 7504 micromirrors. The metal multilayer stack of aluminum–chrome–aluminum (Al–Cr–Al) is deposited by means of electron-beam evaporation, followed by second lithography and deposition of

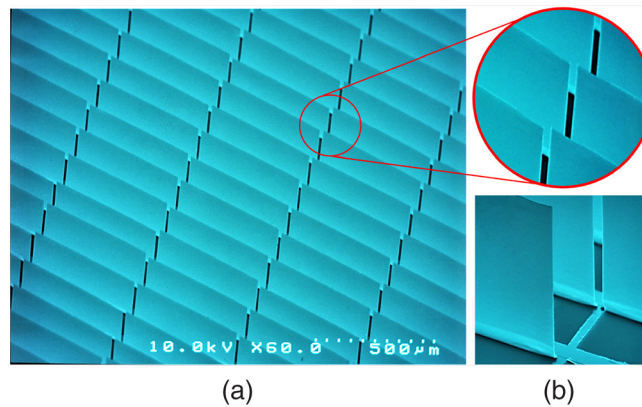


**Fig. 6** (a) SEM micrograph of vertically standing, flat micromirror array with an inset of magnified area. (b) SEM micrograph of the hinge area showing the vertical fully open state (opening angle of  $\sim 90$  deg).

aluminum layer at the mirror area as stress compensation layer. Upon removal of the sacrificial photoresist layer in lift-off process and the subsequent drying process, the micromirrors will be released and standing vertically with planar mirror area (Fig. 6). Normally, the opening angle for  $U = 0$  V is about 90 deg from the substrate surface. Since electrical field lines are oriented vertical to the metal layers and the forces act vertical to the mirror plane, even mirrors with angles deviating from 90 deg in both directions for  $U = 0$  V (initial state) are actuatable.

#### 4 Experimental Characterization

The important characteristics of micromirror array are the actuation voltage, the response time, and the transmission. These three parameters are defined based on the comparison with alternative and existing shutter concepts (as summarized in Table 1) as well as the applicable regulation and standards. Our current transmission of  $T_{\min} < 0.01\%$  (closed state) and  $T_{\max}$  of 73% reveals a contrast of 7300, measured with a parallel beam in a goniometer-type setup allowing variable incidence angles. The maximum value was measured for vertical incidence. Currently, we are working toward  $>85\%$  by decreasing the area of the opaque supporting posts and spacers between the mirrors [see Fig. 6(b)]. The actuation voltage is 12 to 40 V. The lowest power consumption of  $0.2 \text{ mW/m}^2$  to keep the mirrors permanently in position is by a factor of 100 or 1000 lower compared to electrochromic (EC) or LCD technologies, respectively. The capacitance–voltage ( $C - V$ ) measurement of micromirror arrays exhibits a hysteretic characteristic (Fig. 7) of micromirror displacement, demonstrating a different threshold voltage of closed ( $V_{\text{close}}$ ) and open state ( $V_{\text{open}}$ ). This allows a lower potential (holding voltage,  $V_{\text{hold}}$ ) needed to maintain the closed state ( $V_{\text{close}} > V_{\text{hold}} > V_{\text{open}}$ ).

As for subfield addressing of micromirror arrays, the selective actuation of a specific subfield is achieved by exploiting the hysteretic characteristic. A distinct difference between closing and opening voltage is needed for the selective actuation since the nonselected subfields in the same rows and columns will also be addressed together with the selected subfields. This is a known disadvantage of PM scheme and also one of the reasons for AM scheme with incorporation of TFT as nonlinear switch is utilized. Various combinations of potential differences across the top and bottom electrodes are applied with multichannel waveform generator so that the potential difference in a selected subfield is higher than the closing voltage  $V_{\text{close}}$ , whereas the potential differences of nonselected subfields are maintained lower than the  $V_{\text{close}}$  (Fig. 8). This approach requires voltage sources capable of handling the number of connections needed (8 channels in case of a  $4 \times 4$  passive matrix arrangement). A more efficient method can be achieved via multiplexing based on the response time of micromirrors or by a driver circuit with high-voltage shift register and control signal from a microcontroller. The preliminary design of such driving circuit has been established with successful functional test and will be published in a separate article. Depending on the mirror design, the measured response times are varied and

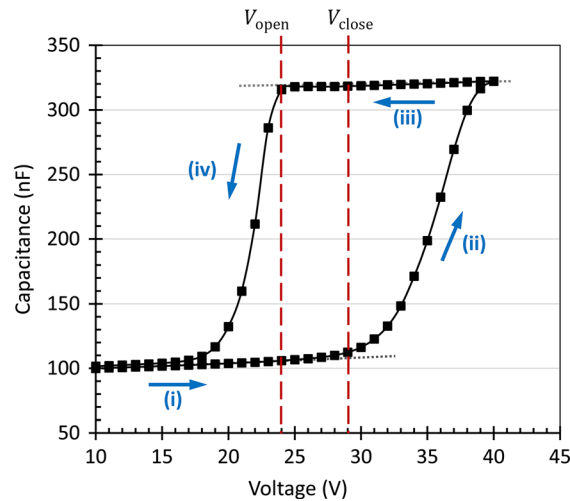


**Fig. 7** Typical  $C - V$  curve from actuation of a  $10 \text{ cm} \times 10 \text{ cm}$  sample at room temperature: (i) the mirrors remain in their default open position when the applied voltage is less than the closing threshold; (ii) mirrors are closing when actuation voltage exceeds the closing threshold; (iii) once the mirrors are fully closed, they will remain in the closed state as long as the voltage applied is more than the opening threshold, thus allowing a lower voltage needed to maintain the closed state; and (iv) mirrors are opening when the voltage is reduced beyond the opening threshold.

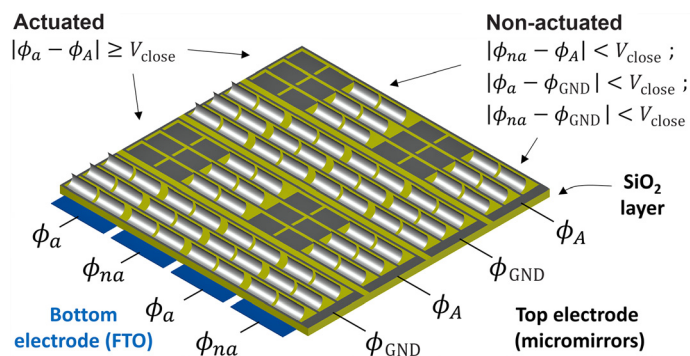


**Fig. 8** Schematic diagram a  $4 \times 4$  passive matrix arrangement in a  $10 \text{ cm} \times 10 \text{ cm}$  array module. The selective actuation is achieved via combination of various potential differences and exploiting the known opening and closing voltage characteristic. Figure modified from Ref. 30.

are in the range of lesser than  $200 \mu\text{s}$ —much faster than the current alternatives (for example, EC and LCD/SPD systems), which commonly range in seconds to even hours in unfavorable conditions. A detailed explanation and comparison between our micromirror concept and existing alternatives can be found in our previous publication.<sup>6</sup>

## 5 Laboratory and Function Demonstrators

The fabricated micromirror arrays have been mounted in double or quadruple insulation glazing separated by spacers. Before sealing the panes with butyl, the ambient air was exchanged by Argon. Thus the MOEMS arrays are in inert gas atmosphere. The mounting has been performed in our laboratories as well as in the production line of the company Energy Glas GmbH using a modern standard industrial window module fabrication process. Figure 9(a) depicts a cross section of a quadruple insulation glazing module with micromirror arrays. A laboratory demonstrator has been constructed using four  $10 \times 10 \text{ cm}^2$  micromirror arrays in a modern quadruple insulation glazing filled with Ar using the above-mentioned standard industrial fabrication

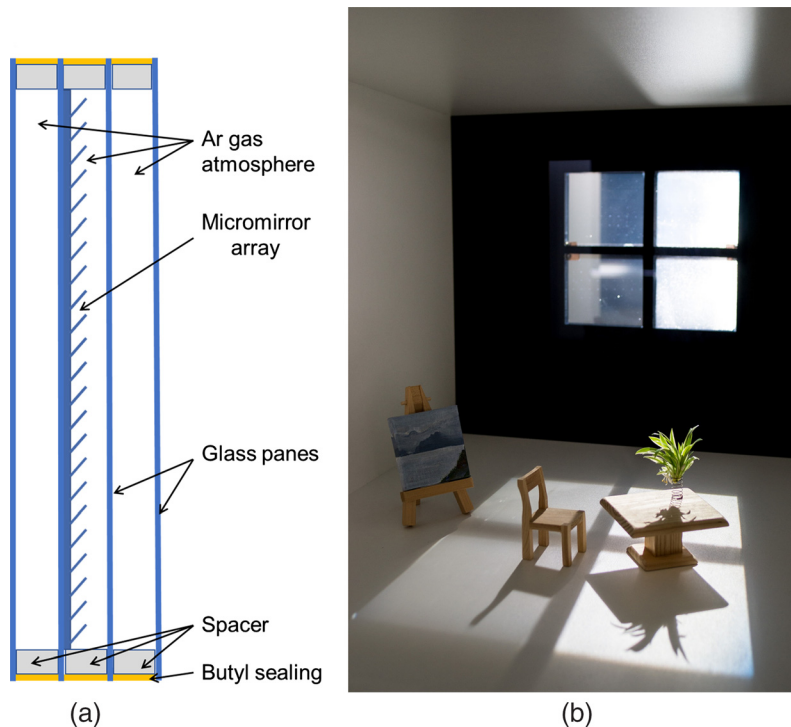


**Fig. 9** (a) Illustrated construction of micromirror arrays in quadruple insulation glazing and (b) the installation in a doll house as lab demonstrator, visualizing the tailored light guiding and ambience control in a room.

process. Subsequently, this smart window of 400 cm<sup>2</sup> active area has been inserted in a doll-house (Fig. 9). The successful fabrication of a lab demonstrator is an important milestone in the research and development of micromirror arrays for smart window applications. Even though in small scale, the lab demonstrator is a proof of concept—verifying the feasibility as well as the compatibility with standard module manufacturing process of commonly used isolation glazings.

Subsequently, the functionality has been improved by the implementation of subfield addressing. Subfield addressing in the micromirror array enables customized solutions of open and closed areas in a single-window module and smart personal environments. Such important function is necessary to facilitate personalized ambient lighting. Our function demonstrator reveals subfield addressing by segmentation of each of the 4 arrays into 16 addressable subfields via a 4 × 4 passive matrix arrangement. These four subfield arrays were mounted in a double insulation glazing, resulting in a total of 64 addressable subfields in an active area of about 400 cm<sup>2</sup> and subsequently installed as a smart window in another dollhouse (Fig. 10). The fabrication process is further simplified by the mounting adapter to assist in the placement of the four subfield modules with their own respective connection lines [Fig. 10(a)]. This is achieved by embedding a designated connection circuit and contact pins in the mounting adapter. The illumination pattern on the ceiling and floor of the dollhouse in Fig. 10(b) is an example of light guiding variation and tailored ambience lighting in a room via selective actuation of subfields. The subfield actuation is executed by applying potential differences between the four top and four bottom electrodes, as shown in the schematic diagram in Fig. 8. With the closing and opening voltage values ( $V_{\text{close}}$  and  $V_{\text{open}}$ ) known from experimental characterizations, a specific subfield can be in state of actuated (closed), nonactuated (open), or in between (up to the limits given by the pull-in effect), depending on the potential difference between the top and bottom electrode. Selection of different subfield combinations can be achieved by applying a different set of potential differences across different rows and columns, or by time multiplexing.

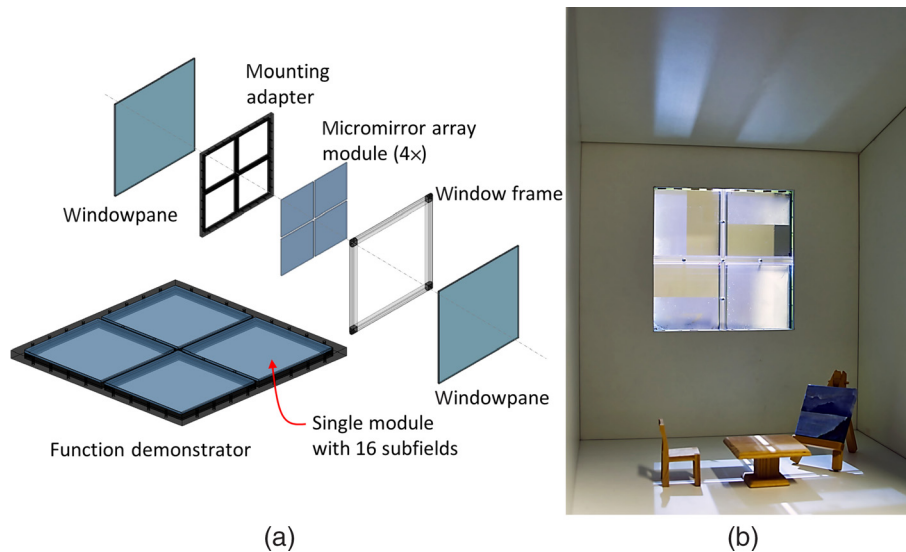


**Fig. 10** (a) Explosion drawing of the function demonstrator consisting of four micromirror array modules housed in double insulation glazing using standard industrial fabrication process and parts. (b) An example of personalized room lighting in a dollhouse by selective actuation of specific subfields, where a variation of guided light on the ceiling can be observed. Link to actuation video: Ref. 31.

## 6 Reliability and Lifetime Studies

Packaged MOEMS can experience harsh environmental situations such as ultraviolet (UV), visible, or IR radiation; weather conditions such as humidity, rain, ice, snow, wind, and sand-storm; and temperature changes. Moreover, the lifetime of surfaces in technical systems are subject to vibrations and mechanical shocks. Hence, quality control is essential in MOEMS design and technological fabrication to experimentally deduce the long-term reliability and lifetime pertaining to the aforementioned conditions. Rapid aging tests are conducted to gain as much information as possible about potential failure. Such practice enables a legitimate estimation of mean-time-to-failure rates, lifetimes, and reliability data by manufacturers for customer specifications. Aging tests reveal a failure probability as a function of time (in units of several years), the so-called bathtub curve, which is characterized by a time interval at the beginning showing a decreasing failure rate, followed by a long-time interval characterized by a constant failure rate, and a time interval of reincreasing failure rates at the end. For example, burn-in tests are performed for semiconductor lasers<sup>32</sup> to directly reach the long second interval of low failure rates. Thus for a product at a distinct time after its delivery, the manufacturer as well as the customer are fully aware of the current probability of failure.

Micromachined devices are packaged for practical use and sometimes they are even sealed in inert gas. Our micromirror arrays for active light steering in smart windows are sealed in Ar atmosphere inside the insulation glazing (at least double glazing), as depicted in Fig. 3(a) and detailed in our previous publications.<sup>6,7</sup> Insulation glazing are filled with noble gases (argon or krypton) since single-atomic gases exhibit the best thermal insulation properties next to vacuum. Such arrangements support the reliability of micromirror arrays enormously due to the absence of moisture and oxygen that could harm the metallic surfaces of the mirrors in the long term. Therefore, the remaining reliability issues that could cause material and structural failure are narrowed to (i) vibrations and mechanical shocks, (ii) long-term electrostatic actuations, (iii) extreme temperatures and sudden temperature variations, and (iv) UV radiation. Experiments on all four issues have been performed and have already shown very promising results. In this paper, the first three are presented.

### 6.1 Vibrations and Mechanical Shocks

In order to experimentally simulate rapid aging in that field, programmable external mechanical actuators are used for long-term periodic vibrations at different frequencies or for programmable

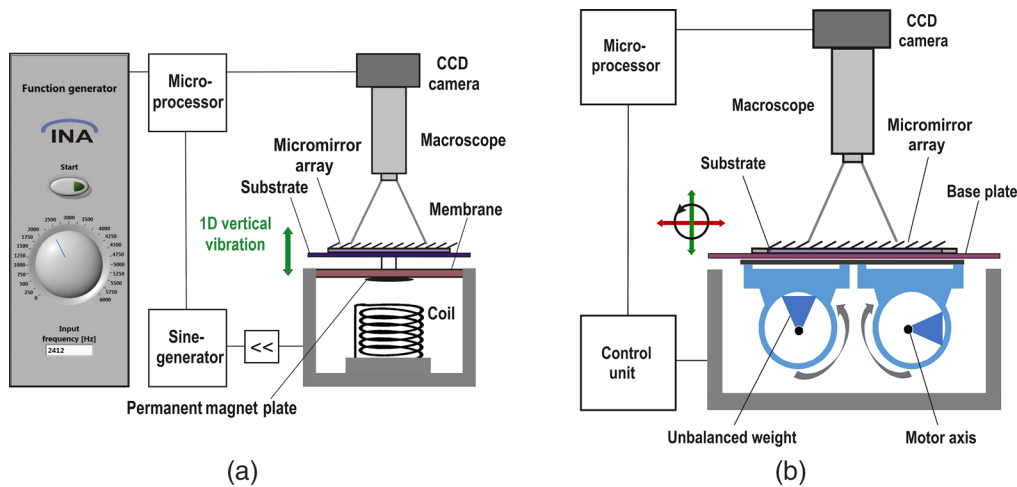


**Fig. 11** (a) Reliability set-up for 1D vertical vibration (green double arrow). The variable frequency is defined by the sine generator, amplified, and translated via the coil into an alternating magnetic field driving the permanent magnetic plate attached to the bottom of the membrane. (b) Reliability set-up for 2D vibration. Two intentionally unbalanced electromotors (phase shift of  $\pi/2$  shown here) drive the base plate in a vertical (green double arrow) and one lateral direction (red double arrow).

shock sequences with different temporal acceleration profiles. Here we report on 1D and 2D vibrations. Our 1D vibrations are oriented vertical to the substrate plane. Our 2D vibrations are oriented in the two directions vertical to the hinge axis. This reveals higher stress to the mirrors than lateral actuations parallel to the hinge axis.

### 6.1.1 Long-term vertical 1D vibration

Here the micromirror samples have been placed in horizontal position and undergo a forced oscillation under sinusoidal vertical external mechanical excitation [Fig. 11(a)]. The sample holder is fixed to a membrane equipped with a thin permanent magnetic plate at the bottom. The alternating magnetic field of the coil below excites the membrane to forced oscillations at variable frequencies. The oscillation frequency is generated by a sine generator that, after amplification ( $\ll$ ), feeds the coil. The setup enables a frequency variation in the range of 0 to 6 kHz.

### 6.1.2 Long-term 2D vibration

For the external mechanical excitation, two electromotors with unbalanced axis are used [Fig. 11(b)]. The two masses used for the unbalanced rotation can be adjusted at variable phase shifts (0 to  $2\pi$ ). The micromirror arrays are placed in horizontal position and undergo forced oscillations under sinusoidal external mechanical excitation up to frequencies of 100 Hz. Although the adjustable frequency range is limited, the test setup enables very high amplitudes and accelerations up to 8.5 g. The experiments were performed with a phase shift of  $2\pi$  at 60 Hz. Using an optical macroscope (resolution of  $8\ \mu\text{m}$ ), images were recorded in intervals of several days to document any visible changes on the samples. To ensure that always the identical sample position and the same section are inspected, samples showing characteristic arrangements of defects have been selected for the tests.

During long-term 1D or 2D vibration, not a single-mirror got damaged and no failure was observed, demonstrating high reliability and long lifetimes. The experimental parameters are summarized in Table 2.

## 6.2 Long-Term Electrostatic Actuation and Amplitude Modulation Response Measurements

By placing a light source on one side of the sample, the light transmitted through the micromirror arrays is detected by a fast photodiode on the opposite side and displayed as a transient intensity

**Table 2** Experimental parameters of 1D and 2D vibration tests. The samples differ in the heterostructure design of the micromirrors but have the same lateral dimensions ( $150\ \mu\text{m} \times 400\ \mu\text{m}$ ). All samples survived the vibrations without any damages and physical changes.

| Sample no. | Type | External actuation frequency (Hz) | Total actuation time (h) | No. of interrupts for photos | Total no. of photos |
|------------|------|-----------------------------------|--------------------------|------------------------------|---------------------|
| 1          | 1D   | 2500                              | 671                      | 11                           | 13                  |
| 2          | 1D   | 1769                              | 1226                     | 18                           | 20                  |
| 3          | 1D   | 2412                              | 1327                     | 19                           | 21                  |
| 4          | 1D   | 3278                              | 13,634                   | 64                           | 66                  |
| 5          | 1D   | 278                               | 720.7                    | 14                           | 16                  |
| 6          | 2D   | 60                                | 332                      | 2                            | 4                   |

by means of an oscilloscope. Since the transmitted light intensity is related to the deflection angle of the micromirrors by geometrical means, the actuation characteristics of micromirror with increasing frequencies can be examined through observation of the transmitted intensity (amplitude), which is defined by the deflection angle. These types of test measurements are known as an amplitude modulation response experiment. Thus the maximum micromirror deflection was measured as a function of actuation frequency (0 to 10 kHz): a resonance frequency of 3 kHz and a  $-3$ -dB frequency of 6 kHz have been measured. Long-term fatigue tests were performed with electrostatic actuation (electrical excitation) at 3 kHz, at which the robustness and resilience of the micromirrors will be tested under the harshest conditions. Considering the typical average changes of the micromirrors in smart windows initiated by the user, the performed  $10^9$  cycles of opening and closing movement under harshest resonance conditions would correspond in a simple approximation to lifetimes of several hundred years. Such outcome further concludes that with the utilization of micromirror array-based smart windows, lifetimes of at least 40 years can be extrapolated. Our samples are fabricated without antistiction coating and no stiction of micromirrors are observed, as evidenced in the actuation video<sup>31</sup> (Fig. 10).

All our tests results conclude that no failure of our smart glass is expected during transportation and installation process, as well as in long-term use. The influence of gravity and inertia forces is minimized in the microworld, thus nearly eliminating material fatigue. This is treated in detail in our previous papers,<sup>6,7</sup> in conclusion of that: with shrinking mirror sizes (down-scaling), the relative importance of electrostatic forces used for the actuation grows on the expense of the strongly vanishing gravity and inertia forces responsible for material fatigue. This is an important and encouraging result, demonstrating sustainability, and robustness of MOEMS technology on surfaces, under the assumption that the elements are sufficiently miniaturized.

### 6.3 Reliability under Extreme Temperatures and Sudden Temperature Variations

For these reliability studies, micromirror modules in double insulation glazing have been mounted in a climate chamber. The wiring is fed through via cable entries. Measuring the capacity as a function of the actuation voltage (CV), we could always check the actuation operation. For different temperatures between  $-80^\circ\text{C}$  and  $+120^\circ\text{C}$ , proper actuation was measured without any failure. For these extreme temperatures, the micromirrors show fast closing and reopening movement and the butyl sealing survived. In comparison, EC glazings require more than 1 h for switching in the range below  $0^\circ\text{C}$ .

Temperature changes between day and night and sudden changes in sun radiation can limit the device lifetime. This transient thermal stress was simulated by multiple fast temperature cycles ( $0 \rightarrow +80 \rightarrow 0 \rightarrow +80^\circ\text{C} \dots$ ) over a full week. The pane modules show no failure, revealing high reliability, and long lifetime.

## 7 Comparison of MOEMS Smart Glass with Other State-of-the-Art Shading Systems

*Conventional outdoor and indoor blinds (macromechanical systems).* Outdoor blinds are efficient to block solar heat in summer but are vulnerable for wind and cannot be used above the 7th floor due to wind condition. Indoor blinds are much less efficient since absorbed radiation heats up the blinds, acting as undesirable radiation heaters in summer. Blinds are subject to high mechanical wear (material fatigue), thus shortening their lifetime. Moreover, these systems have a quite limited user benefit. Although reflective blinds integrated between the panes of the insulation glazing windows might be a good compromise, such concept is well behind our smart window in terms of adjustability and light transmittance.

*Intelligent glazing for room lighting and temperature control.* Unlike conventional systems, intelligent glazing is active. Some available switchable glazings, namely polymer dispersed liquid crystals, polymer stabilized liquid crystals, and suspended particle devices (SPD), are based on active aligning of molecules. PDLC is based on light scattering and can only be switched between a transparent and a translucent (milky) state, which is in fact mainly suitable for indoor applications. SPD and EC technologies are based on light absorption, which leads to temperature increase inside windows, and thus undesired radiation heating effects toward the room in summer. For all systems, the transmission contrast  $T_{\max}/T_{\min}$  is very different: 6 to 60 for EC, 1.5 for PDLC, 60 for SPD, and 7300 for our MEMS arrays. Electrochromic technologies cannot be produced without undesired coloring (not color neutral) and are very slow (switching time in range of an hour under  $-5^{\circ}\text{C}$ ). Compared to our technology, both competing types (light absorbing and scattering) do not have additional benefits of personalized light steering. Note that in case of power failure, PDLC and SPD windows are not transparent and EC windows may be not fully transparent—or in the worst case nearly opaque. Nontransparent windows in emergency cases are potentially very dangerous. Our smart micromirror glazing can avoid these disadvantages and risks. Note that tri-stable scattering type liquid crystal displays have been developed by Wang et al.,<sup>33</sup> capable of retaining the transparent and opaque states without voltage. In future, this could reduce energy consumption, enormously. As of present, they are unfortunately still not color neutral and not available on larger area.

In general, our smart MEMS glazing is by far more progressive and successful in energy saving in lighting, air condition, and heating systems: (i) in summer, illuminating only the area close to present persons minimizes the incoming heat, (ii) vertical metal mirrors reflect valuable mid-IR back into the room at night in winter, (iii) heating with solar IR in winter, and (iv) avoiding artificial light in many cases. In our previous publication,<sup>6</sup> we compared our smart innovation with other shading systems.

## 8 Summary

Our MOEMS micromirror arrays for active smart windows have the following advantages: (i) much higher actuation speed and much larger operating temperature range than electrochromic systems, (ii) insensitivity to wind in contrast to external active sun blinds, (iii) low-power consumption in comparison with systems based on all other concepts, (iv) no heating of the window in contrast to thermochromic, chemochromic, and electrochromic systems, which are based on absorption, (v) color neutrality in contrast to electrochromic technologies, and (vi) the most important advantage of a huge  $\text{CO}_2$  saving potential up to 30% and an energy saving potential up to 35%, if applied in smart buildings. The energy saving results from savings in artificial lighting, air conditioning, and heating generated by the novel smart glazing based on micromirror arrays. The electrostatic actuation only requires a minimum in electrical energy: the low-power consumption of as low as  $0.2 \text{ mW/m}^2$  and actuation voltages of as low as 12 V. A lab demonstrator was reported as well as a function demonstrator revealing subfield addressing with 64 individual fields.

Rapid aging tests of micromirror structure were performed to study reliability, demonstrating sustainability, robustness, and long lifetimes of the micromirror arrays for future application. The micromirrors have endured and survived through the most demanding test conditions (mechanical vibrations  $>12.000 \text{ h}$  at 3278 Hz, extreme temperatures  $-80^{\circ}\text{C}$  to  $+120^{\circ}\text{C}$ ,

multiple temperature cycles, and long-term electrical actuation for  $>10^9$  open close cycles). These results consequently validate the reliability of micromirror arrays—in future applications in active windows—far beyond 40 years, as well as their robustness during transportation, installation, and against all the vibration influences in buildings.

## Acknowledgments

The author would like to thank J. Schmid, G. Xu, C. Woidt, H. Wilke, H. Luo, M. Khan, J. Krumpholz, A. Friedrichsen, T. Nurjahan, N. Körte, S. Liebermann, S. Baby, A. Nandakumar, T. Thomas, M. Smolarczyk, Shashank, V. Viereck, A. Jäkel, J. Clobes, F. v. Waitz, D. Gutermuth, and I. Kommallein for the fruitful discussion and technological support; Energy Glas GmbH in Wolfhagen for the technical assistance in housing in insulation glazing; as well as DBU (Nos. AZ23717, AZ20012/189, and AZ35501), EU MEM4WIN, EU NEXT BUILDINGS, and BMBF (No. 13N14517) for financial support.

## References

1. A. Aksyuk et al., “Beam-steering micromirrors for large optical cross-connects,” *J. Lightwave Technol.* **21**(3), 634–642 (2003).
2. L. Lin and E. Goldstein, “Opportunities and challenges for MEMS in lightwave communications,” *IEEE J. Sel. Top. Quantum Electron.* **8**, 163–172 (2002).
3. C. Pu et al., “Client-configurable eight-channel optical add/drop multiplexer using micro-machining technology,” *IEEE Photonics Technol. Lett.* **12**(12), 1665–1667 (2000).
4. W. Duncan et al., “Dynamic optical filtering in DWDM systems using the DMD,” *Solid-State Electron.* **46**, 1583–1585 (2002).
5. B. Ballard et al., “‘Steering’ light with texas instruments digital micromirror device (DMD)—past, present and future,” *SID Symp. Dig. Tech. Pap.* **47**(1), 28–31 (2016).
6. H. Hillmer et al., “Optical MEMS-based micromirror arrays for active light steering in smart windows,” *Jpn. J. Appl. Phys.* **57**(8S2), 08PA07 (2018).
7. M. S. Q. Iskhandar et al., “Development of optical MEMS-based micromirror arrays for smart window applications: implementation of subfield addressing and reliability measurements,” in *Jahrbuch Oberflächentechnik*, T. Sörgel, Ed., Vol. **75**, pp. 93–107, Leuze Verlag, Bad Saulgau, Germany (2019).
8. S. Manzanera et al., “MEMS segmented-based adaptive optics scanning laser ophthalmoscope,” *Biomed. Opt. Express* **2**(5), 1204 (2011).
9. T. Bifano, “Adaptive imaging MEMS deformable mirrors,” *Nat. Photonics* **5**(1), 21–23 (2011).
10. N. Doble and D. R. Williams, “The application of MEMS technology for adaptive optics in vision science,” *IEEE J. Sel. Top. Quantum Electron.* **10**(3), 629–635 (2004).
11. G. Zhu et al., “Flatness-based control of electrostatically actuated MEMS with application to adaptive optics: a simulation study,” *J. Microelectromech. Syst.* **15**(5), 1165–1174 (2006).
12. E. Schlam, J. Finch, and J. Koskulics, “Highly reflective electrostatic shutter display,” in *Proc. Int. Disp. Workshops*, Sendai, Japan (2017).
13. S. Ilias et al., “Programmable optical microshutter arrays for large aspect ratio microslits,” *Proc. SPIE* **7099**, 70992D (2008).
14. C. G. Kalt, “Electro-static device with rolling electrode,” U.S. Patent No. 4,094,590A (1976).
15. C.-H. Kim and S. Hong, “Study on the reliability of the mechanical shutter utilizing roll actuators,” in *Proc. IEEE 24th Int. Conf. Micro Electro Mech. Syst.*, Cancun, Mexico, pp. 501–504 (2011).
16. M. Pizzi et al., “Electrostatically driven film light modulators for display applications,” *Microsyst. Technol.* **10**(1), 17–21 (2003).
17. P. Roux et al., “Fem modelling of an electro-optical micro-shutter,” *Sens. Actuators A* **119**, 1–7 (2005).
18. B. Lamontagne et al., “The next generation of switchable glass: the micro-blinds,” in *Proc. Conf. Glass Perform. Days*, Tampere, Finland (2009).

19. P. Schalberger, S. A. A. Nusayer, and C. Raichle, "Parallel fabrication for integration of electronic and microelectromechanical systems," *SID Symp. Dig. Tech. Pap.* **47**(1), 731–734 (2016).
20. K. Mori et al., "A MEMS electrostatic roll-up window shade array for house energy management system," *IEEE Photonics Technol. Lett.* **28**(5), 593–596 (2016).
21. B. Lamontagne et al., "Review of micro-shutters for switchable glass," *J. Micro/Nanolithogr. MEMS MOEMS* **18**(4), 040901 (2019).
22. S. H. Goodwin-Johansson et al., "Reduced voltage artificial eyelid for protection of optical sensors," *Proc. SPIE* **4695**, 451–458 (2002).
23. D. Langley, S. Rogers, and L. Starman, "Fabrication studies for scaling photonic MEMS micro-shutter designs," *Proc. SPIE* **7096**, 70960G (2008).
24. C. Kim, K. Jung, and W. Kim, "A wafer-level micro mechanical global shutter for a micro camera," in *Proc. IEEE 22nd Int. Conf. Micro Electro Mech. Syst.*, pp. 156–159 (2009).
25. K.-S. Lim et al., "Wide bandwidth reflective microshutter blind panel for transparent organic light-emitting diode display," *SID Symp. Dig. Tech. Pap.* **47**(1), 1389–1391 (2016).
26. K.-H. Lee, J. Chang, and J.-B. Yoon, "High performance microshutter device with space-division modulation," *J. Micromech. Microeng.* **20**(7), 075030 (2010).
27. S. A. Al Nusayer et al., "TFT integrated microelectromechanical shutter for display application," *SID Symp. Dig. Tech. Pap.* **49**(1), 498–501 (2018).
28. P. M. Alt and P. Pleshko, "Scanning limitations of liquid-crystal displays," *IEEE Trans. Electron Devices* **21**(2), 146–155 (1974).
29. K. Blankenbach, A. Hudak, and M. Jentsch, "Direct drive, multiplex and passive matrix," in *Handbook of Visual Display Technology*, J. Chen, W. Cranton, and M. Fihn, Eds., pp. 417–437, Springer, Cham (2012).
30. M. S. Q. Iskhandar et al., "Design, fabrication and characterization of subfield addressing in micromirror arrays for smart window applications," in *Int. Conf. Opt. MEMS and Nanophotonics*, Daejeon, South Korea, pp. 192–193 (2019).
31. M. S. Q. Iskhandar et al., "Subfield actuation," [https://hessenbox.uni-kassel.de/getlink/fiU9sznXf2qE7ZxbshiJ1m6x/Subfield\\_Actuation.mp4](https://hessenbox.uni-kassel.de/getlink/fiU9sznXf2qE7ZxbshiJ1m6x/Subfield_Actuation.mp4) (2020).
32. F. R. Nash et al., "Selection of a laser reliability assurance strategy for a long-life application," *AT&T Tech. J.* **64**(3), 671–715 (1985).
33. C.-T. Wang et al., "A stable and switchable uniform lying helix structure in cholesteric liquid crystals," *Appl. Phys. Lett.* **99**, 041108 (2011).

**Hartmut Hillmer** received his PhD from Stuttgart University in 1989 on electronic transport in semiconductor QWs and his habilitation degree from TU Darmstadt in 1996 on the QW material system AlGaInAs. He worked at Research Center German Telekom from 1989 to 1999 on semiconductor lasers, and NTT Optoelectronic Laboratories, Japan, in 1991. He has been a professor since 1999 and a board member since 2016 of Graduate Academy at the University of Kassel. He received "European Grand Prix for Innovation Awards" in 2006. His research fields are microsystem technology, nanosensors and actuators for smart personal environments, and active windows.

**Mustaqim Siddi Que Iskhandar** received his BEng degree in 2012 in mechatronics and microsystem technology from Heilbronn University of Applied Sciences and his MS degree in 2014 in electrical and electronics engineering from the University of Kassel. He has worked in semiconductor and oil and gas sectors before pursuing his PhD in 2017 at the Institute of Nanostructure Technologies and Analytics (INA). His research concentrates on the implementation of subfield addressing and establishment of cost-effective, large-area lithography process for the fabrication of micromirror arrays.

**Muhammad Kamrul Hasan** received his MSc degree in electrical communication engineering in 2020 from the University of Kassel, Germany. His field of research was in the optimization of the structuring process of TCO used in micromirror arrays. Currently, he is working as a researcher at INA while pursuing his PhD at the same time. His current field of research focuses on the further development of micromirror arrays for improved daylight guiding functionalities.

**Sapida Akhundzada** received her BSc degree in 2017 and MSc degree in 2019 both in nanoscience from the University of Kassel, Germany. From 2017 to early 2020, she was working at Photonik Inkubator GmbH, Germany, on the optimization of fabrication process of micromirror arrays. Currently, she is pursuing her doctorate degree in the field of functional thin films at the Institute of Physics of the University of Kassel.

**Basim Al-Qargholi** received his MSc degree in electrical communication engineering in 2011 and his PhD in 2016 both from the University of Kassel, Germany. His main area of study was the fabrication of microstructure elements used for daylight guiding. He was working as a researcher at INA from 2011 to 2017, and subsequently as an application engineer to fabricate a microsystem for daylight guiding at Photonik Inkubator GmbH, Germany.

**Andreas Tatzel** received his PhD in 2018 from the University of Kassel on the development and fabrication of micromirror arrays as a lab demonstrator. He was working at the INA from 2012 to 2016, heading a research group on micromirror arrays from 2015 onward. His research focus was investigation of residual stresses in thin-film layer stacks and their application in curvature design for micromirrors. Currently, he is working at X-FAB Semiconductor Foundries AG, Erfurt.